DOI: 10.13009/EUCASS2022-4867
9TH EUROPEAN CONFERENCE FOR AERONAUTICS AND SPACE SCIENCES (EUCASS)

Design of a Flush Air Data Sensing System for the Hypersonic Flight Experiment HEXAFLY-INT

Johannes Riehmer, Ali Gülhan** and Johan Steelant****

** Research Scientist, DLR Institute of Aerodynamics and Flow Technology, Supersonic and Hypersonic Technologies Department, Cologne, Germany, johannes.riehmer@dlr.de*

*** Head of Department, DLR Institute of Aerodynamics and Flow Technology, Supersonic and Hypersonic Technologies Department, Cologne, Germany, ali.guelhan@dlr.de*

**** ESA ESTEC, Flight Vehicles and Aerothermodynamics Engineering Section TEC-MPA, P.O. Box 299, Noordwijk, Netherlands, Johan.Steelant@esa.int*

Abstract

The HEXAFLY-INT flight vehicle is a small-scale flight demonstrator of a supersonic passenger aircraft [8,9]. In order to determine the flight angles, Mach number and altitude for this vehicle a set of pressure sensors can be used to derive this data. In the frame of this study such a system, usually called Flush Air Data Sensing system (FADS), was designed and adapted to the constrains imposed by the vehicle shape of HEXAFLY-INT. Different theoretical, analytic and numerical approaches from local inclination method to numerical simulations were used to optimize sensor positions for the flight path of HEXAFLY-INT. Afterwards these different approaches was assessed and benchmarked against each other. In the second part of this work different algorithms are investigated to determine the flight properties for simulated inputs and were analyzed in terms of accuracy and real-time performance.

Nomenclature

ADS	Air Data System
AoA	Angle of Attack
AoB	Angle of Sideslip
ANN	Artifical Neuronal Network
CFD	Computation Fluid Dynamics
FADS	Flush Air Data System
LUT	LockUp Table
locInc	Local Inclination (Method)
WTT	Wind Tunnel Test

α	Angle of attack
β	Angle of sideslip
c_p	Stagnation pressure
M	Mach number
p	Pressure
Re	Reynolds number

1. Introduction

1.1 Overview

An Air Data Systems (ADS) is a commonly known system of multiple (pressure) sensors which are processed in order to get the angle of attack, angle of sideslip, Mach number and pressure (altitude). It is used in wind tunnels in form of a 5-hole probe or in commercial/military aircrafts. In Figure 1 the basic principle underlying data scheme of an ADS is shown.

DOI: 10.13009/EUCASS2022-4867

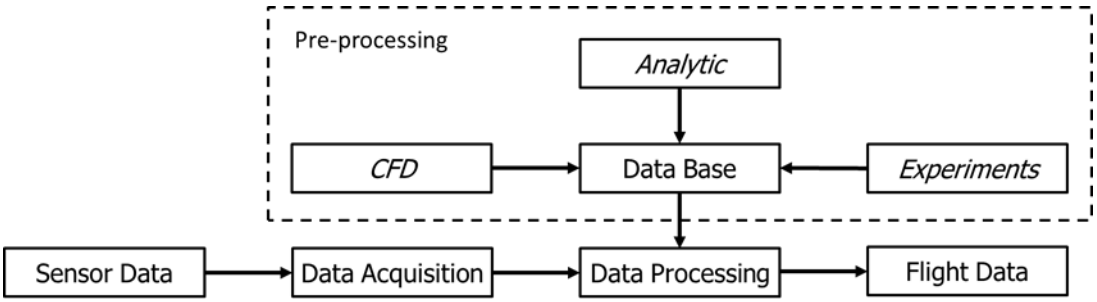

Figure 1: Sketch of an ADS

The classical designs are mostly applicable for subsonic configurations. For supersonic and hypersonic applications an ADS needs to be integrated in the shape of the vehicle in order to avoid negative local aerodynamic and aerothermodynamic effects on the vehicle. By using flush mounted pressure sensors this system is extended to the Flush Air Data Sensing systems (FADS). Due to the absence of any obstructions into the flow no shocks or local hot spots are induced to the system. The downside of such system is that it is tailored to the specific vehicle and requires dedicated calibration and qualification. Also, it cannot be guaranteed the same accuracy of the tailored FADS to the commercial subsonic and transonic ones.

Flush Air Data Sensing systems were used in different applications like supersonic military aircrafts (NASA) [7], reentry capsules [5] and Hypersonic aircrafts [1][12]. DLR tested and evaluated this technology recently for SHEFEX II [10] and ROTEX-T [3]. In contrast to the majority of these applications the presented configuration is not axis-symmetric and therefore an alternative design and evaluation processes had to be invented.

Within this study a design approach for a FADS tailored to the HEXAFLY-INT flight vehicle is introduced. Hereby the work is split into four major parts:

- General design, layout and concept of the FADS within the vehicle including sensor positions
- Generation of multiple data bases based on analytic, numeric and experimental methods
- Algorithm development and implementation
- Evaluation, verification and uncertainty analysis

1.2 Constrains

The methods and constrains presented in this paper apply to a very specific use-case which is derived from the HEXAFLY-INT flight vehicle and therefore are not suited for direct application on other vehicles or shapes. Also, in order to reduce the design space, the system is adapted and (in a certain degree) optimized for a nominal flight condition of Ma=7 and 31km (1000Pa) altitude. For off-design conditions an uncertainty study is performed. In order to reduce the parameter space further only nominal angle of attack of -10° to 20° and sideslip between -10° and 10° were calibrated.

Finally, a principle parameter space splitting approach was used. Earlier investigation showed that the determination of angle of attack and sideslip generally have a significant smaller uncertainty than the uncertainties in Mach number and pressure. For real flight application altitude and velocity are available via GPS and IMU data in a higher accuracy than it can be derived from the FADS and by use of this data the uncertainty can reduced. Therefore, in this work is focused on the determination of the flight vector and Mach number and pressure (altitude) determination get a lower priority.

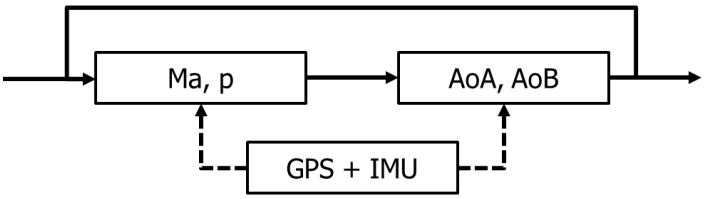

Figure 2: Optimizer cycle for HXI-FADS

DOI: 10.13009/EUCASS2022-4867

2. Methods

2.1 Flow Simulation

Two general different models were used to predict or calculate the flow around the nose of the HEXAFLY-INT vehicle. The analytic and fast local inclination method as the most robust and simple model was used as baseline. In order to compare the results with alternative more detailed numerical flow fields the DLR flow solver TAU were used.

Local Inclination Method

The local inclination-method used in this paper determine the local angle of attack and sideslip of the surface at the pressure measurement position and assumes a wedge flow with the local inclination of the combined angles. For negative angles of the surface Prandtl-Mayer-Expansion equation was used while for to high angles the oblique shock equation was replaced by the normal shock equation. The resulting implicit equation was solved using the secant method and gives for any combination a valid solution which is the main advantage over other approaches which have incomplete databases (experimental data) or suffer from numerical problems like singularities (CFD).

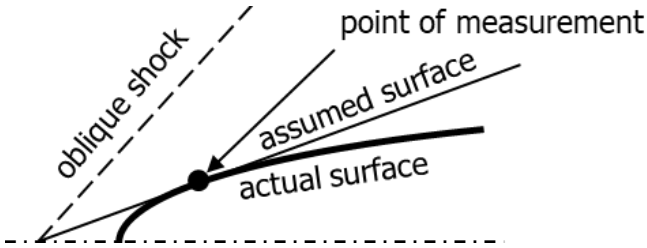

Figure 3: Local inclination method

An important implication of this flow modulation is that the calculated pressure coefficient is independent from the static flow conditions in terms of pressure and temperature; respectively there is no Reynolds number dependency. This implies that neither the Mach number nor the ambient pressure can be calculated directly from a measured pressure and a known pressure coefficient and is always a combination of these both parameters.

Numerical Simulations

For numerical simulations the DLR flow solver TAU was used. It is a CFD software package for solving Euler or Reynolds-averaged Navier-Stokes (RANS) equations for compressible and incompressible flow [6]. In the frame of this work the basic simulations where performed using the Euler module due to restricted computational resources. Since Euler calculations are also Reynolds number independent like the local inclination method the Mach number and ambient pressure cannot be derived independently.

In order to get a data including a Reynolds number dependency for dedicated points along the trajectory viscous simulation were performed assuming laminar boundary conditions. From other studies [11] on the HEXAFLY-INT vehicle the boundary layer transition was expected to occur further downstream and the nose is for the investigated part of the trajectory always laminar.

2.2 Artificial Neuronal Network

Artificial neuronal networks are computational models based on the structure and functions of a biological neuronal network. In this study an artificial neuronal network approach is used to determine the flow parameters from a set of sensors by train the model on data from different databases. This means the ANN is used as a fast and easy inter- and extrapolation method of the database data. The framework used here was Python based Keras frontend [2] with Tensorflow [?] as backend.

3. FADS Design

The design process consists of two mayor parts. The first part was the sensor placement on the vehicle which is fundamental in terms of model definition and all further work. While the second part focuses on the data processing, algorithms and analysis descript in the next chapter. Since the full design of the FADS and the data processing algorithm was not available at the beginning of the project a “hands-on” approach was used to define the sensors and sensor positions and is descripted in the next section.

The design of the FADS for HEXAFLY-INT was rather an iterative design process under certain constrains than a straight forward optimization. In order to reduce the design, afford it was performed only to a flight condition close to

DOI: 10.13009/EUCASS2022-4867

the stationary flight condition of HEXAFLY-INT already descript in the introduction. A hard constrain was to have no measurements in the leading edge in order to avoid problems during the manufacturing of the vehicle. Other drawbacks would have been a strong dependency of the measurement on the flow vector itself due to the relatively big size of the pressure port in comparison to the leading edge, transition triggering and aerothermal effects. Beside this constrain two main assessments were performed in order to get potential positions of the sensors and will be explained further:

Sensitivity on flow vector variations

For this assessment multiple flow fields for different angle of attack, sideslip and Mach numbers were performed using the Local Inclination Method. In Figure 4 exemplary data is plotted for angles of attack and sideslip showing the difference in the pressure coefficient in comparison to flow with no angle of attack and sideslip.

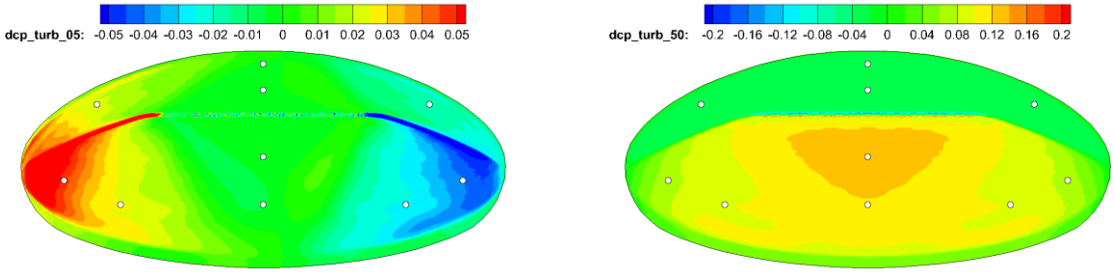

Figure 4: Difference in pressure coefficient of Euler simulation for different α and β in comparison to level flight

In order to get a clear signal (pressure) for a deflection of the vehicle the sensors should be placed in red or blue regions of these plots. For a sideslip variation these regions on the sides of the vehicle are favorable while for angle of attack variation the bottom part along the centerline is better.

Sensitivity on viscous effects

In Figure 5 the difference between a frictionless Euler simulation and a laminar flow simulation is shown for different angle of attacks and sideslip. The red and blue regions show differences between the two simulations and indicate a stronger derivation between the two models. As seen in Figure 5 the derivations are 40x lower than the derivations from the slight flight angle variations in Figure 4 indicating the lower influence of the friction model. This shows on one hand that Euler simulation and viscous simulation are quite similar and the influence of friction on the pressure coefficient is very low. This qualifies the Euler simulation to be valid and sufficient but on the other hand shows also that Reynolds number influence cannot resolved with pressure measurements prohibit the parameter separation of Mach number and ambient pressure (see 2.1).
From this assessment no dedicated sensor positions could be derived from the viscous effect assessment.

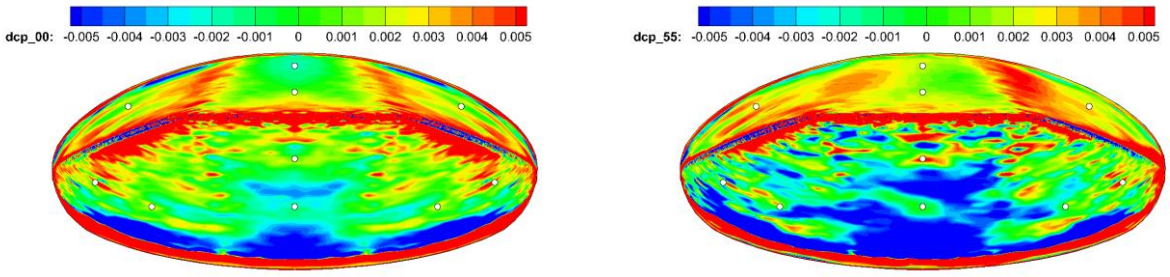

(a) α=0° and β=0° (b) α=5° and β=5°

Figure 5: Difference between laminar and Euler Simulations

Beside these considerations some further points were considered in order to define the positions of the sensors:

- A symmetric distribution was chosen in order to make use of some symmetric simplifications.
- Along the symmetry line of the HEXAFLY-INT vehicle the surface is flat for the first few centimeters (no curvature) and therefore has less 3d-flow effects and is mainly depending on the angle of attack (and not sideslip) and therefore from special interest.
- (Additionally) Measurements on the flat surface on the symmetry line have the same local inclination and will show similar pressure coefficient. A derivation of two measurements with the same local inclination but different positions upstream can be used to better determine the flow conditions in terms of Mach number and pressure.

DOI: 10.13009/EUCASS2022-4867

- In order to be redundant 10 sensors were used.

The final positions of the sensors are shown in the picture below with the used numbering within this study and the position in the y-z-plane.

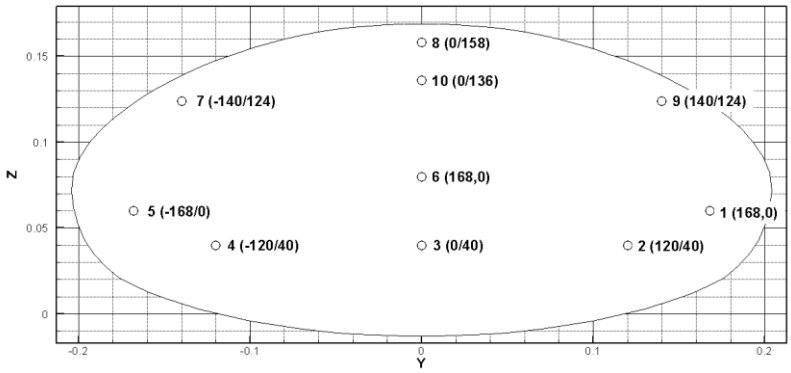

Figure 6: Sensor positions

4. Analysis Algorithms

This chapter will descript the two used models of getting the flow properties out a measurement using the data obtained from the analytic or CFD database. Due to the non-axially symmetric shape of the nose simplifications using the Taylor-Maccoll equation are not possible which rules out a direct evaluation of flight parameters from the measurement data. Therefore, the first approach is the lookup table approach which is already used in the previous chapter on verification and model assessment. The second approach uses an artificial neural network which is trained by the database we got from our models.

4.1 Look-Up Table (LUT)

As already descripted in the introduction the concept for the algorithm is split in the evaluation of Mach number and pressure and Angle of attack and sideslip separately. Whereas the second part (AoA and AoB determination) has a higher priority since a higher accuracy can be achieved here. In order to underline this hypothesis a simple uncertainty approximation is performed and plotted in Figure 7 and Table 1. Hereby the local inclination method was used to determine the pressure derivation for each sensor of the 10 sensors for different angle of attack, sideslip, Mach number and pressures according to the following equation and the reference condition.

$$\Delta \boldsymbol{p} = \sum\left(\boldsymbol{p_i}(\boldsymbol{p}, \boldsymbol{M}, \boldsymbol{\alpha}, \boldsymbol{\beta}) - \boldsymbol{p_i}(\mathbf{1000}\ \boldsymbol{Pa}, \mathbf{7.0}, \mathbf{0°}, \mathbf{0°})\right)^{\mathbf{2}} \quad \textbf{(1)}$$

These resulting picture shows a color map which can be interpreted as an uncertainty distribution where same colors have the same uncertainties. The main findings are also collected in Table 1 as well and show that for an uncertainty of ±0.5° in angle of attack the equivalent uncertainty in angle of sideslip is ±1.7°. The corresponding uncertainty of pressure is ±860 Pa which is equivalent to an uncertainty of ±3.2 km@30km. Also, the Mach number shows a significant uncertainty. But the Mach number and high are correlated as it can be seen in Figure 7. The strange shape of the "uncertainty" of Mach number and pressure (resp. altitude) stem from the independency of the pressure coefficient database on the pressure.

Table 1: Uncertainties for LUT

	AoA	**AoB**	**p**	**M**	**H**
Uncertainties	±0.54°	±1.72°	±860 Pa	±2.4	±3.2 km

DOI: 10.13009/EUCASS2022-4867

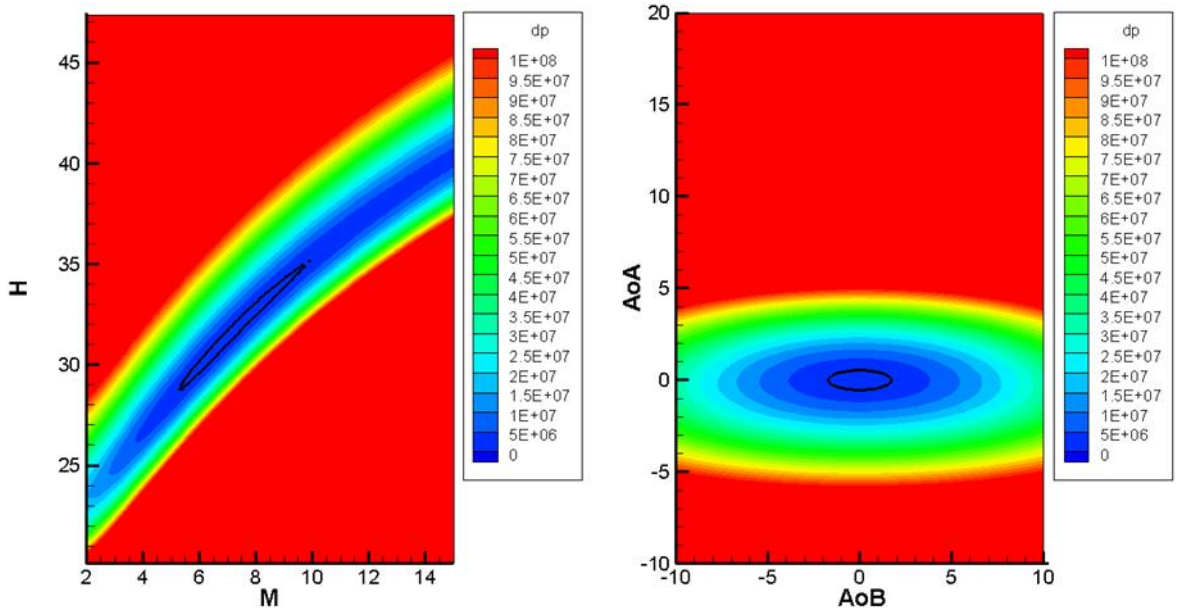

Figure 7: Uncertainty analysis for reference condition

The principle algorithms will work with the same equation and try to minimize the upper equation. Whereas the pressures are normalized with the stagnation pressure and the pressure coefficient instead of the measured pressure is used. Also, the pressure was replaced by the Reynolds number because most underlying databases use Reynolds analogy and are not based on a pressure and allow a better interpolation and extrapolation. The upper equation is therefore modified in the following form and a minimum has to be found by an algorithm. The w value is added to give a weighting of the individual sensor and is set to 1 for all cases in this document but can be used to tweak the accuracy of the algorithm.

$$\Delta \boldsymbol{c_p}(\boldsymbol{Re}, \boldsymbol{M}, \boldsymbol{\alpha}, \boldsymbol{\beta}) = \sum \boldsymbol{w_i}\left[\boldsymbol{c_{p,meas,i}} - \boldsymbol{c_{p,db,i}}(\boldsymbol{Re}, \boldsymbol{M}, \boldsymbol{\alpha}, \boldsymbol{\beta})\right]^2 = \boldsymbol{min} \quad \textbf{(2)}$$

The equation is usually solved by definition of the boundary of the parameter space followed by the calculation of any parameter combination in the 4-dimsensional parameter space and plotting the calculated delta pressure coefficient. By finding the minimum the most likely flow conditions can be approximated. Since the data of the database was usually not stored for each point of the domain interpolation has to be applied. Due to complexity and computational intense of 4-D interpolation and with the approach shown in Figure 2 the algorithm was split into two serialized 2-D interpolation algorithms which could also use in an iterative loop to increase accuracy. For interpolation a cubic interpolation was used for the flight angle determination was used while for the Mach number and Reynolds number linear interpolation was used due to the lack of grid points. For databases without Reynolds number dependency the interpolation was simplified to 1 dimensional interpolation.
It should be mentioned that the normalizing of the equation to dimensionless variables (M, Re, c_p) requires functions which perform parameter conversions ($p \rightarrow c_p$, $p \rightarrow Re$, …) which themselves requires some approximation or assumptions and especially need an initial assumption to get the algorithm to work.

4.2 Artificial Neuronal Network

The artificial network approach was in terms of complexity and effort much less demanding than the “Lookup Table” approach. In order to train the ANN a train data set has to be extracted from the individual database. Therefore, randomly picked entries of the database were simple transferred into the train database with application of Gaussian noise on the individual sensor data. A slightly variation was performed for the experimental data where not the (approximated) database was used. Instead the original input data was used since the interpolation and extrapolation should be performed by the ANN algorithm and not by the analytic approximation descript in 5.2.
With the train data the network was trained and benchmarked with accuracy of the train algorithm which was usually higher than 90%.

DOI: 10.13009/EUCASS2022-4867

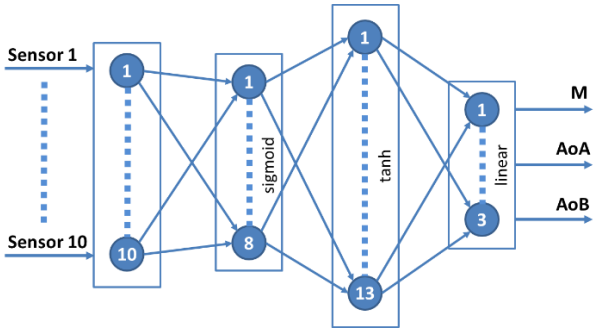

Figure 8: Schematic of the FADS-ANN

The network itself consists of 10 input knots using the sensor data several hidden layers and an output layer mapping the output directly on the flow parameters. In Figure 8 the schematic of the used feedforward ANN with 2 hidden layers is shown. The detailed structure was found by a brute-force algorithm combining randomly different layers with different activation functions and knots and benchmarking them in terms of accuracy. One of the best performing algorithms with the fewest knots was chosen. The performance was around 95%.
As seen in the graph the algorithm was simplified by dropping the Reynolds number influence. This was done because the indecency or lack of datapoints in most databases in terms of the Reynolds number.

5. Databases

For this study databases were generated based on basically three different models. Since these databases had different structure a data postprocessor had to be created which transfer the data of the different models into a common data format which the different analysis algorithm could process. In the current case it has been a simple table with the four parameters Re, M, α and β and the pressure coefficient for each sensor of the specified condition.

5.1 Local Inclination Database

The analytic approach was the baseline of this study and first used the Newton flow theory for hypersonic flow. During this study this was slightly improved by use of a local inclination model using oblique shock equation to get the pressure coefficient on the individual sensor position (see Chapter 2.1.1).
The advantage of this approach is the simplicity which allows calculating the conditions for any set of supersonic conditions within a reasonable amount of time and without running into numerical problems. The downside is the higher uncertainty of this method.

5.2 Experimental Database

The experimental approach is detailed descript in the complementary paper. Several experiments have been performed in the H2K and TMK wind tunnels at the DLR in Cologne for Mach numbers between 2 and 8 for different angle of attack and sideslips.
The experiments created polar curves which measured the individual sensor data while angle of attack and sideslip (or both) varied continuously. In Figure 9 the measured pressure coefficient for sensor 1 for 6 different experimental runs at Mach 7 are shown as black lines. In the x and y axis the corresponding angle of attacks and sideslip are plotted. As it can be seen in this graph the curves are insufficient to represent the whole domain in terms of angle of attack and sideslip.
In order to get a valid and useful data base for further analysis the data obtained from the experiments needed to be interpolated and extrapolated to the whole investigated domain. In order to do so and the observation of the curved data behavior a quadric surface description of the plane created by the polar curves with the following equation was assumed (see also colored plane in Figure 9):

$$c_{p,i}(\alpha,\beta) = a_i \cdot \alpha^2 + b_i \cdot \beta^2 + c_i \cdot \alpha + d_i \cdot \beta + e_i \cdot \alpha \cdot \beta + f_i \quad (2)$$

The equation holds for a single sensor for a dedicated Mach number and pressure. Since the coefficient a to f where not known a least-square regression method from the Python SciPy module based on Levenberg-Marquardt algorithm was used. The input to the algorithm was the measured data and the corresponding angle of attack and sideslip provided by the wind tunnel measurements.

DOI: 10.13009/EUCASS2022-4867

The advantage of this interpolation method is the simplification by approximation of the whole domain with only 6 parameters. This way the whole domain can be descripted analytically and therefore this interpolation was also partially applied by the other methods. Another advantage is the use of faster algorithm when an analytic description of the problem is possible, which will be explained in the algorithm chapter.

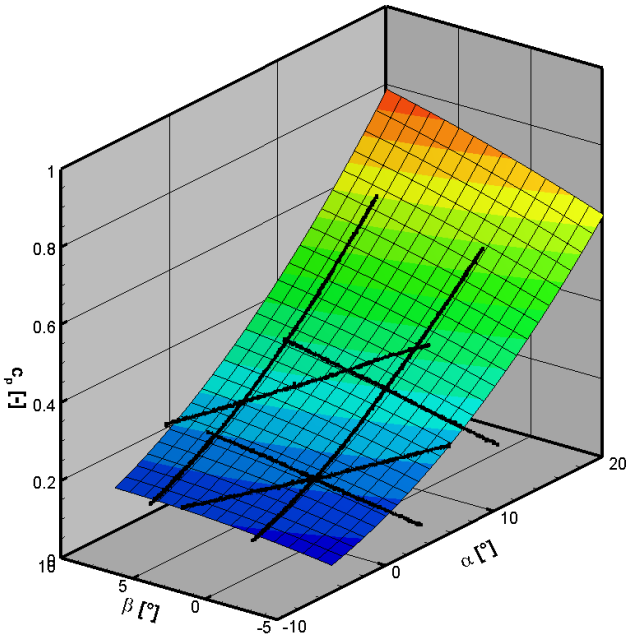

Figure 9: Pressure curves and plane for sensor 1 at Mach 7

5.3 CFD Database

The numerical approach used the DLR Tau solver descripted in the “Methods” section. For Mach numbers from 2 to 8 Euler simulations for each Mach number were performed starting with a 0.5 mil. cells mesh using an automated script with automated adaptation which increased the number of cells to 1.5 mil. For each Mach number 48 combinations of angle of attack and sideslip were calculated which are shown in Figure 10 leading to a total amount 336 simulations. In Figure 10 the simulation grid for one Mach number is plotted. For each simulation the surface pressure distribution was stored and the sensor pressure was extracted afterwards using a script probing data from the surface data. Due to symmetry only positive angle of sideslip had to be evaluated.

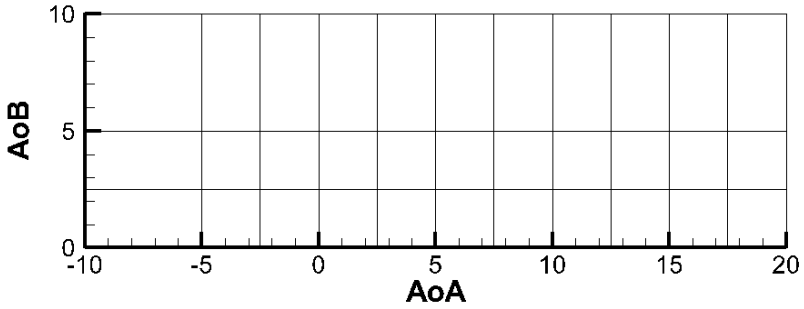

Figure 10: Parameter grid for numerical simulation

For Mach 7 these simulations were also performed assuming laminar flow around the nose of the vehicle and the flight conditions for stationary flow with an isothermal wall of 600 K. Herby a mesh with 2.5 mil. cells were used without adaptation.

5.4 Comparison

In order to compare the databases, the left plot in Figure 11 shows the differences between the analytic approach (Local Inclination), the Euler simulation (CFD Euler), the laminar simulation (CFD lam) and the experiment (Experiment)

DOI: 10.13009/EUCASS2022-4867

whereas the experiment was chosen to be the baseline of the comparison. In the figure the difference in the pressure coefficient for sensor 1 is plotted for different angle of attack and sideslip at Mach 7 at 31km. The sensor 1 for visualization is used since it is expected that the strongest 3d-effects are seen here. All data shown here used the quadric interpolation method for visualization.

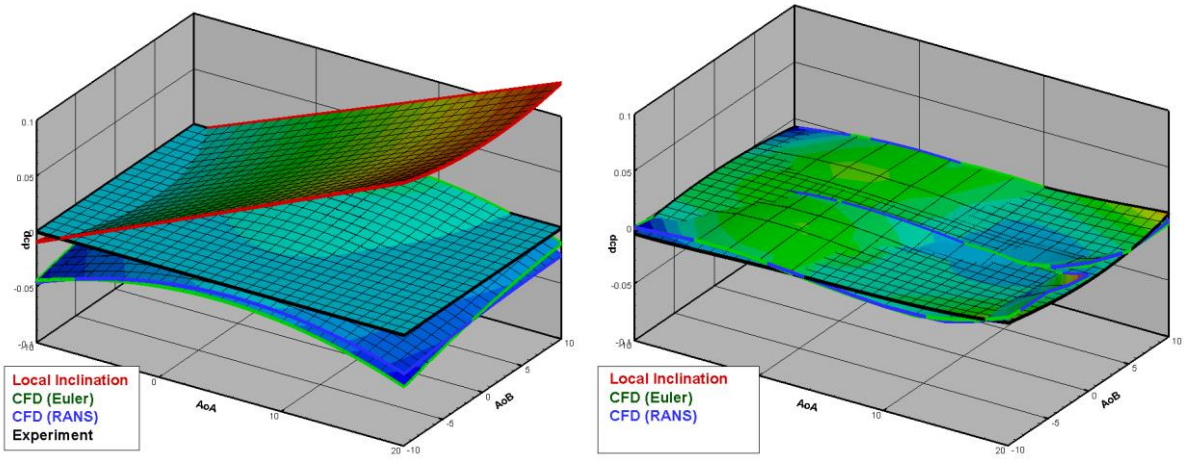

Figure 11: Differences between the various databases and uncertainty in the interpolation method

As expected the local inclination method has the biggest difference from the experimental data especially for high angle of attacks. The numerical simulation shows very similar results with only small differences between each other, but also strongly derivate from the experimental data.
On the right side of Figure 11 the difference between interpolation shape and database data is shown for the local inclination method and the CFD simulations. It can be seen that the differences are quite small in comparison to the left plot (same z axis). In Table 2 the difference between the individual sensors in terms of pressure coefficient is shown on comparison while in Table 3 the difference between the raw data and the interpolated data of each method is shown. All data refers to the standard derivation. The tables are shown in order to give an overview on the uncertainties of the individual models and the interpolation.

Table 2: Differences in pressure coefficient between various databases

	SUM	CP1	CP2	CP3	CP4	CP5	CP6	CP7	CP8	CP9	CP10
Newton	***0.03255***	0.05910	0.04221	0.03916	0.03848	0.05712	0.01225	0.02177	0.02166	0.01821	0.01559
CFD (lam)	***0.01358***	0.01162	0.01246	0.01708	0.02075	0.01277	0.01632	0.01305	0.01239	0.00815	0.01123
CFD (el)	***0.01381***	0.01352	0.01301	0.01734	0.01726	0.01315	0.01823	0.01200	0.01316	0.00914	0.01125
WTT	***0.00000***	0.00000	0.00000	0.00000	0.00000	0.00000	0.00000	0.00000	0.00000	0.00000	0.00000

Table 3: Differences in pressure coefficient between raw data and interpolation

	SUM	CP1	CP2	CP3	CP4	CP5	CP6	CP7	CP8	CP9	CP10
Newton	***0.00350***	0.00173	0.00223	0.00263	0.00223	0.00173	0.00263	0.00575	0.00513	0.00575	0.00513
CFD (lam)	***0.00494***	0.00247	0.00385	0.00817	0.00550	0.00244	0.00518	0.00484	0.00572	0.00425	0.00702
CFD (el)	***0.00444***	0.00249	0.00293	0.00520	0.00480	0.00225	0.00684	0.00529	0.00483	0.00322	0.00659
WTT	***0.00427***	0.00353	0.00375	0.00367	0.00343	0.00304	0.00399	0.00594	0.00563	0.00449	0.00524

The uncertainties caused by the interpolation are (depending on the basis) significantly smaller 10%-40% than the uncertainties between the different models. Which allow the use of this interpolation for this assessment but also offer the potential for further improvements.

6. Verification and Model Assessment

Verification and benchmark were performed on different wind tunnel runs. In order to simplify representation and visualization it is focused on a single run at the reference condition at Mach 7 in the H2K wind tunnel. In order to make

DOI: 10.13009/EUCASS2022-4867

it comparable to the flight condition the pressure data was scaled to an ambient pressure of 1000 Pa (respectively 31.0 km) assuming constant cp.

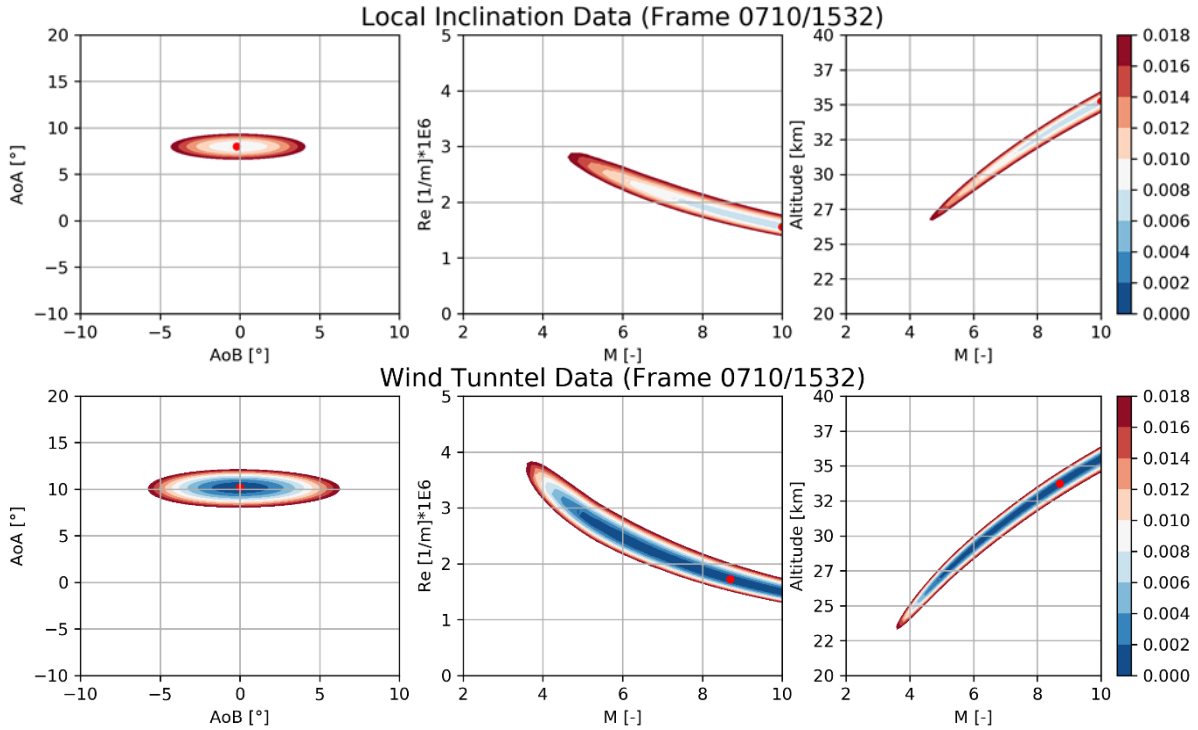

Figure 12: Derived flight condition for the local inclination method (top) and wind tunnel (bottom) databases

In Figure 12 the results for the 710's data point of the wind tunnel run is shown for the lockup table approach using the "local inclination" and "wind tunnel" database. Shown is a difference between measured data and database data in terms of $(\Delta c_p)^2$ while values above 0.02 are clipped. For each database an AoA-AoB plot and a Ma-Re plot is shown. The latter one is also transferred in a Ma-Altitude plot in the 3rd graph. The plots use the same color-scaling for $(\Delta c_p)^2$ which can be interpreted as (dimensionless) probability or likelihood of the specific parameter whereas a low $(\Delta c_p)^2$-value corresponds to a high probability. Iso-surfaces indicate similar probabilities and give a hind on the uncertainty of the specific parameter.

Again, the figures already show the same shapes already descripted in Figure 7: a circular shape for the AoA-AoB plot with a higher uncertainty for the AoB value and a strange shape for the M-Altitude plot with a higher uncertainty which is connected to the stagnation pressure.

The comparison between the wind tunnel and Local Inclination database show a general comparable shape of the uncertainties while the $(\Delta c_p)^2$-value is generally higher for the Local Inclination based analysis indicating a higher uncertainty. The obtained angle of attack from the local inclination database is significant less than the actual 10°-angle for this specific data point whereas the wind tunnel database predicts the angles quite correct. For the Ma-Re/Altitude plot a wide field of Mach numbers with corresponding altitudes (resp. pressure or Reynolds numbers) are possible and the minimum is found more in the region of M=8 but with high uncertainties. Assuming a known flight altitude with corresponding pressure of 1000 Pa the uncertainty can be significantly reduce and is M=7±0.5 for $(\Delta c_p)^2$=0.02. This is quite small considering that the data bases did not include Reynolds number effects. In Figure 13 the results for the inviscous and laminar flow simulations are shown. Even the Mach number and altitude are calculated correctly whereas the laminar simulation gives slightly better results.

DOI: 10.13009/EUCASS2022-4867

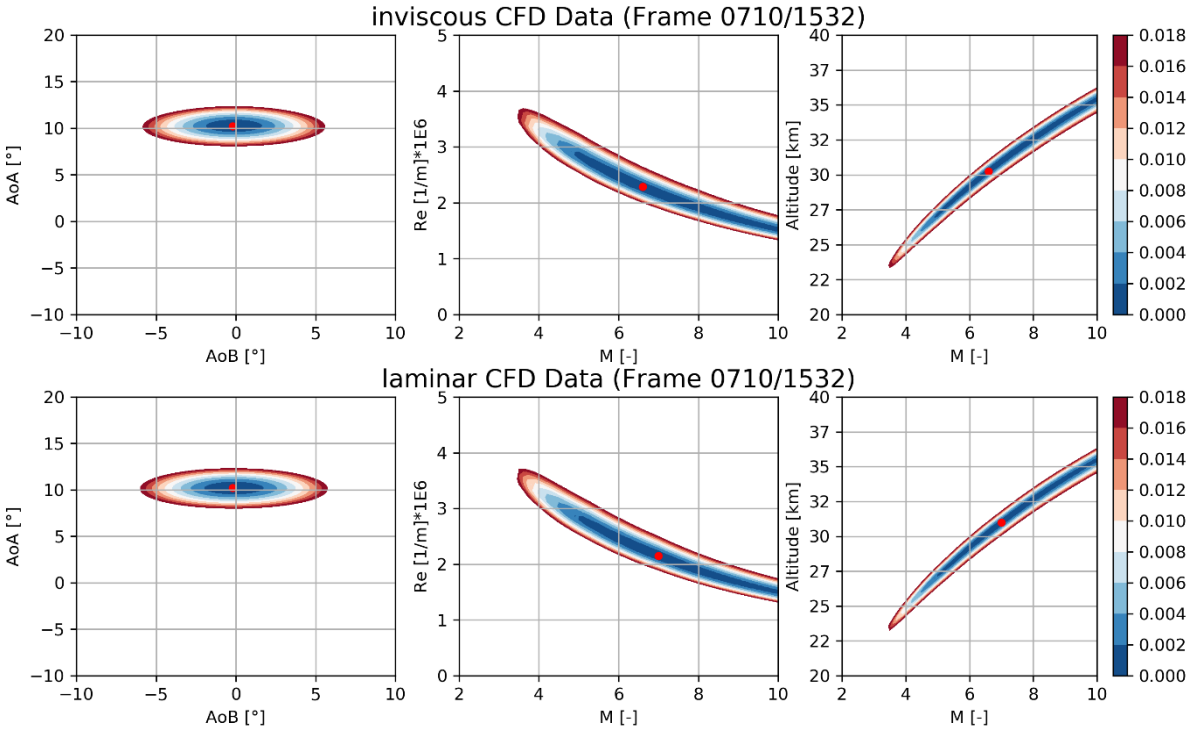

Figure 13: Derived flight conditions for Euler (top) and laminar flow (bottom) based databases

Finally, in Figure 14 a polar curve produced for the experimental run from the previous analysis is shown and evaluated for each individual measurement step. In order to show the discrepancies between the different approaches and databases the difference between the calculated and actual angle of attack is also plotted on the lower graphs. On the left side the lookup table approach is shown while on the right side the ANN approach is visualized. The general trend is replicated with all databases for both approaches whereas the local inclination-based database shows the highest derivation from the actual data. The shape of the LUT approach shows a saw tooth like shape which is due to the discretization of the computational domain which was set to 0.2° due to performance issues. In contrast the ANN approach shows some oscillations which are most likely caused by the chosen activation functions of the ANN.

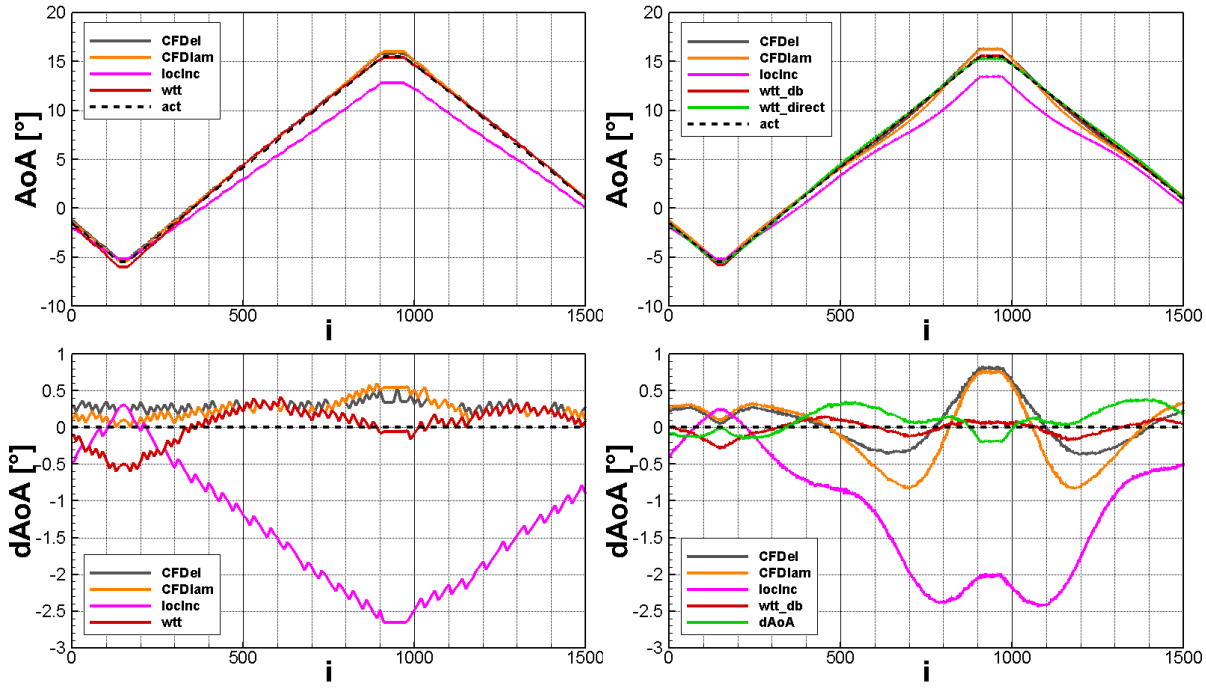

Figure 14: Comparison between LUT (left) and ANN (right) approach

DOI: 10.13009/EUCASS2022-4867

In Table 4 the arithmetic mean and standard deviation of the difference between the calculated and the actual angle of attack is collected for the experimental run is shown. Again, the deviation of the local inclination is the highest with over 1° whereas the deviation of the other databases is below 0.3°. By comparing the ANN with the LUT approach the accuracy (mean) is 3 times better with an uncertainty below 0.1° whereas the standard deviation is 3 times higher for the ANN.

Table 4: Arithmetic mean and standard deviation of the different approaches and databases

		WTT (direct)	WTT (interpol.)	Local Inclination	CFD (inviscous)	CFD (laminar)
Mean [°]	LUT		0.04	-1.36	0.30	0.25
	ANN	0.10	-0.01	-1.16	0.08	-0.04
RMS ["²]	LUT		0.24	0.84	0.07	0.14
	ANN	0.17	0.10	0.85	0.31	0.45

Generally, both algorithms perform comparable well and give comparable results. The advantage of the ANN is the performance which significantly outruns the classical approach even when considering the learning phase. The advantage of the LUT approach is the possibility of a better uncertainty analysis and a general more scientific approach which gives a better understanding of the underlying correlations.
The differences between the databases are relatively small except for the local inclination-based type. It is hard to say if the differences between the results and the actual value are caused by the databases, the algorithms itself or the tweaking parameters of the algorithms.

7. Conclusion

Within this study a FADS concept of the HEXAFLY-INT flight vehicle was designed and descripted. Two different data analysis approaches based on a lookup table (LUT) and on an artificial neuronal network (ANN) have been elaborated, tested and benchmarked. The both approaches show similar results and accuracies for a test case of a wind tunnel run. The LUT approach is hereby in favor for a scientific post flight evaluation of data while the ANN is lightweight in the implementation and is advantageous for real-time application onboard a flight vehicle. The underlying databases have been created by means of simple analytic approximations, numerical inviscous and laminar simulations and experimental data. The different databases lead to similar results showing consistency of the data and give thrust into the achieved results. The tools created within this work have been designed modular and expandable in a manner to allow the application for other supersonic and hypersonic flight vehicles.
The presented work is a first step towards a real-time hypersonic and supersonic flight vehicle with arbitrary shapes and shows a promising approach for software and hardware implementation. Nevertheless, a lot of potential have been exposed during the design and implementation of the algorithms. The LUT approach has a significant speed up potential by implementing a gradient algorithm, while an uncertainty assessment is possible with the ANN approach using noise data. The databases itself did not consider viscous effects even partially foreseen in the algorithms and needs to be extended in further work. Finally, the use of an analytic description of the databases offers the possibility in terms of speed, accuracy and will be assessed in further investigations.

References

[1] D Baumann, Ethan, et al. "X-43A flush airdata sensing system flight-test results." Journal of Spacecraft and rockets 47.1 (2010): 48-61.
[2] Chollet, Fran et al. "Keras." https://keras.io. (2015).
[3] Gülhan, Ali. "Main Achievements of the Rocket Technology Flight Experiment ROTEX-T." 21st AIAA International Space Planes and Hypersonics Technologies Conference. 2017.
[4] Martin Abadi, et al. " TensorFlow: Large-Scale Machine Learning on Heterogeneous Systems." (2015).
[5] Schleutker, Thorn, et al. "ExoMars Flush Air Data System: Experimental and Numerical Investigation." Journal of Spacecraft and Rockets 56.4 (2019): 971-982.
[6] Schwamborn, Dieter, Thomas Gerhold, and Roland Kessler. "DLR-TAU Code-an overview." (1999): S4-2.

DOI: 10.13009/EUCASS2022-4867

[7] Sitz, Joel R. F-18 systems research aircraft facility. Vol. 4433. National Aeronautics and Space Administration, Office of Management, Scientific and Technical Information Program, 1992.

[8] Steelant, Johan, et al. "Conceptual Design of the High-Speed Propelled Experimental Flight Test Vehicle HEXAFLY." 20th AIAA International Space Planes and Hypersonic Systems and Technologies Conference. 2015.

[9] Steelant, Johan, et al. "Flight Testing Designs in HEXAFLY-INT for High-Speed Transportation." Proceedings of HiSST (2018).

[10] Thiele, Thomas, Dominik Neeb, and Ali Gülhan. "Post-flight hypersonic ground experiments and FADS flight data evaluation for the SHEFEX-II configuration." Proceedings of 8th European Conference on Aerothermodynamics for Space Vehicles. 2015.

[11] Wagner, Alexander, et al. "Boundary Layer Transition Studies on the HEXAFLY-INT Hypersonic Glide Vehicle." (2019).

[12] Whitmore, Stephen, Brent Cobleigh, and Edward Haering, Jr. "Design and calibration of the X-33 flush airdata sensing (FADS) system." 36th AIAA aerospace sciences meeting and exhibit. 1998.